Proceedings of the 12th International and 52nd National Conference on Fluid Mechanics and Fluid Power (FMFP)
December 19-21, 2025, Nirma University, Gujarat, India

FMFP2025–MPF–089

Computational Modelling of Fluidized Beds: A Comparative Study Under Different Fluidizing Media Using the CFD–DEM Approach

Ravinder Nath[1] and Gaurav Bhutani[1*]

[1]School of Mechanical and Materials Engineering, Indian Institute of Technology Mandi, Himachal Pradesh 175075, India
d22054@students.iitmandi.ac.in; gaurav@iitmandi.ac.in

ABSTRACT

Fluidized beds can be operated with a variety of fluidizing media depending on process requirements. This study aims to provide a deeper understanding of the fluidization behavior of a binary particle system in a three-dimensional cylindrical fluidized bed using two different fluids—air and water—through numerical simulations based on a coupled Computational Fluid Dynamics and Discrete Element Method (CFD–DEM) approach. The system is composed of two different types of spherical particles with equal densities but different diameters (3 mm and 4 mm) arranged in a layered initial configuration. Key hydrodynamic parameters, including bed expansion, pressure drop and mixing behavior are analyzed at various superficial velocity values. Qualitative visualizations and quantitative analyses reveal that water-fluidized beds exhibit more stable and confined particle dynamics due to the higher density and viscosity of the liquid, whereas air-fluidized beds demonstrate greater particle mobility and enhanced bed expansion. The simulated pressure drop values show good agreement with theoretical predictions, with relative errors of 4.08% and 15.6% for the water and air cases, respectively. These results highlight the significant influence of fluid properties on fluidization dynamics and offer practical guidance for the design and optimization of both liquid–solid and gas–solid fluidized bed systems.

Keywords: Granular flow, Fluidized bed, CFD-DEM, Particle mixing.

I. INTRODUCTION

Fluidized beds are widely used in industries such as hydrometallurgy, mineral processing [1], food engineering [2], pharmaceuticals [3], and petrochemicals due to their simple design, uniform solid distribution, efficient fluid–solid contact, and high heat and mass transfer rates. Compared to mechanically agitated reactors, they require lower maintenance costs and offer better product quality. In practice, fluidized beds often handle particles with varying size, shape, and density [4] and operate with different fluidizing media (e.g., air, water), which influence mixing, segregation, and fluid–particle interactions [5]. Understanding these effects is crucial for optimizing system design.

Although several experimental and numerical studies have examined binary fluidized beds with either air or water [6], direct comparisons under similar conditions remain scarce. Existing studies mainly address minimum fluidization velocity, bed expansion, and steady-state pressure drop [7], leaving a gap in understanding the link between fluidizing medium, particle mixing, and flow dynamics.

Moreover, most studies, including the present work, consider only a limited number of particle sizes of equal density. Previous research shows that beds with a broad particle size distribution tend to exhibit a lower minimum fluidization velocity compared to those with a narrow distribution [8], whereas increasing the average particle diameter leads to a higher minimum fluidization velocity [9]. CFD–DEM studies have also highlighted the strong influence of polydisperse particle systems on fluidization behavior and mixing [10]. However, the primary aim of this study is to compare the influence of different fluidizing media on the behavior of binary particle distributions.

Numerical simulations provide detailed particle-scale insights that are difficult to obtain experimentally. Typically two main approaches are available—the Two-Fluid Model (TFM) [11], which treats both phases as continua, and the Computational Fluid Dynamics and Discrete Element Method (CFD–DEM) [2], which models the fluid phase as a continuum and tracks individual particles. While TFM is computationally efficient, CFD–DEM captures particle-scale phenomena such as collisions, trajectories, and fluid–particle interactions, making it particularly suited for mixing studies.

This work employs CFD–DEM to simulate a three-dimensional binary fluidized bed with particles of same density but different diameters. Air and water are used as fluidizing media in the same geometry, with fluidizing velocities adjusted to account for the differing fluid properties, based on the minimum fluidization requirements. The analysis focuses on flow characteristics, bed expansion and mixing behavior to compare gas–solid and liquid–solid systems and assess the influence of the fluidizing medium.

The remainder of this paper is structured as follows. Section II describes the numerical methodology and CFD–DEM framework, while Section III presents model validation against experimental data. Section IV outlines the computational setup, including initial and boundary conditions, numerical setup, and the grid independence study. Section V discusses the simulation results, covering flow behavior and particle-scale analyses. Finally, the main conclusions are summarized in Section VI.

II. METHODOLOGY

This study uses the open-source CFD–DEM framework CFDEM®coupling, which couples the CFD solver OpenFOAM with the DEM engine LIGGGHTS®. The fluid phase is solved using an Eulerian approach, while the solid phase is tracked using a Lagrangian DEM approach. Fluid–particle

interactions are modeled through an interphase drag law.

A. Fluid phase

The fluid phase is described by the volume-averaged Navier–Stokes equations for mass and momentum conservation:

$$\frac{\partial(\alpha_f \rho_f)}{\partial t} + \nabla \cdot (\alpha_f \rho_f \mathbf{u}_f) = 0, \tag{1}$$

$$\frac{\partial(\alpha_f \rho_f \mathbf{u}_f)}{\partial t} + \nabla \cdot (\alpha_f \rho_f \mathbf{u}_f \mathbf{u}_f) = -\alpha_f \nabla p - \mathbf{K}_{sl} + \nabla \cdot (\alpha_f \tau_f) + \alpha_f \rho_f \mathbf{g}, \tag{2}$$

where α_f is the fluid volume fraction, ρ_f the fluid density, $\mathbf{u}_f$ the fluid velocity, p the pressure, $\mathbf{K}_{sl}$ the momentum exchange term between solid and fluid, and τ_f the fluid shear stress tensor.

B. Solid phase

The solid phase is modeled using DEM, tracking individual particles in a Lagrangian framework. Particle motion follows Newton's second law:

$$m_i \frac{d\mathbf{u}_i}{dt} = \mathbf{F}_c + \mathbf{F}_d + m_i \mathbf{g}, \tag{3}$$

$$\mathbf{I}_i \frac{d\omega_i}{dt} = \mathbf{T}_c + \mathbf{T}_{fi}, \tag{4}$$

where m_i is particle mass, $\mathbf{u}_i$ translational velocity, $\mathbf{F}_c$ contact force from particle–particle and particle–wall interactions, $\mathbf{F}_d$ drag force, $\mathbf{I}_i$ moment of inertia, ω_i angular velocity, $\mathbf{T}_c$ torque from tangential contact forces, and $\mathbf{T}_{fi}$ torque due to fluid velocity gradients.

C. Fluid–solid interaction

Fluid–particle momentum exchange is modeled via the drag force:

$$\mathbf{F}_d = \frac{\pi}{8} C_d \rho_f d_i^2 \alpha_f^{2-\beta} |\mathbf{U}_r| \mathbf{U}_r, \tag{5}$$

where C_d is the drag coefficient, d_i the particle diameter, $\mathbf{U}_r = \mathbf{u}_i - \mathbf{u}_f$ the relative velocity between particle and fluid, and β is the interphase momentum exchange coefficient. The Di Felice drag law [2], derived from experimental data for solid suspensions and fixed beds, is used in this work.

III. Model Validation

The model was validated against the fluidization experiments of Khan et al. [4]. The simulation setup replicated the experimental geometry—a cylindrical column 0.7 m high and 0.05 m in diameter—filled with a binary mixture of particles, having a density of $2230\,\mathrm{kg\,m^{-3}}$. Two particle sizes—3 mm and 8 mm—were used, with 120 g of each, initially packed in two layers; finer particles above the coarser ones. Water was injected uniformly from the bottom at a constant superficial velocity U_s, inducing bed expansion.

Five superficial velocities (0.141, 0.149, 0.156, 0.163, and $0.170\,\mathrm{m\,s^{-1}}$) were simulated for 20 s each. Predicted bed expansion and particle distribution closely matched experimental trends. As shown in Figure 1, simulation results exhibited strong agreement with measured expansions across all tested velocities, confirming the accuracy of the CFD–DEM model.

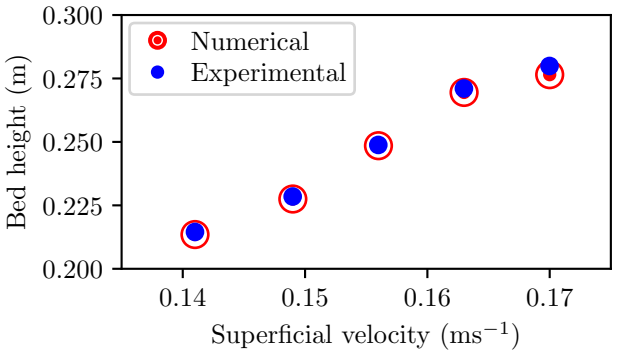

Figure 1: Validation of a binary-mixture solid–liquid fluidized bed under varying superficial velocities.

IV. Computational Setting

The CFD–DEM simulations were configured using the geometry, mesh, initial conditions, and numerical parameters described below.

A. Domain, mesh, boundary and initial conditions

The simulations were carried out in a three-dimensional cylindrical column (D = 0.14 m, H = 0.45 m) containing a binary mixture of cohesionless spherical particles (d_1 = 4 mm, d_2 = 3 mm, ρ_p = $2230\,\mathrm{kg\,m^{-3}}$) arranged in two packed layers, with coarse particles below fine ones and 1 kg of each type. The bottom and top boundaries acted as inlet and outlet, respectively, while the side wall was impermeable. Boundary conditions for velocity and pressure are summarized in Table 1. The system was allowed to settle under gravity before fluid injection. First, a base hexahedral mesh was generated and subsequent local refinements near walls and particle–fluid interfaces were carried out.

Table 1: Boundary conditions for velocity and pressure fields

Property	Inlet	Wall	Outlet
Velocity, $\mathbf{u}_f$	U_s $\mathrm{m\,s^{-1}}$	No-slip	$\frac{\partial \mathbf{u}_f}{\partial n} = 0$
Pressure, p	$\frac{\partial p}{\partial n} = 0$	$\frac{\partial p}{\partial n} = 0$	$p = p_0$

B. Numerical setup

CFD–DEM coupling was implemented by linking OpenFOAM for the fluid phase with LIGGGHTS for particle tracking. Separate time steps were used for fluid ($\Delta t_{\mathrm{CFD}} = 5.0 \times 10^{-6}$ s) and particles ($\Delta t_{\mathrm{DEM}} = 2.0 \times 10^{-5}$ s), with data exchanged at every CFD step. The maximum Courant number was kept below 0.5. Particle and fluid properties, as well as other simulation parameters, are listed in Table 2.

C. Grid independence study

Mesh independence was assessed at $U_s = 3U_{mf}$ where for both water and air cases using coarse (31×31×84), medium (37×39×105), and fine (45×47×126) grids; U_{mf}

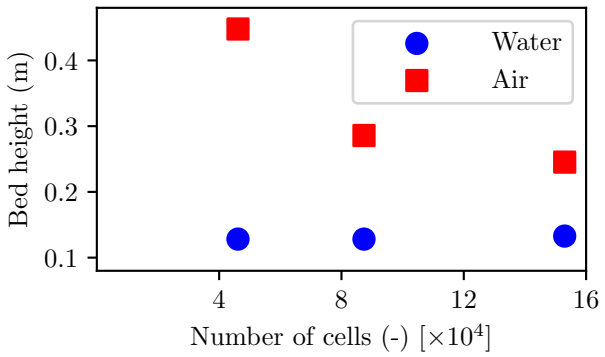

Figure 2: Bed expansion height versus number of cells for both case at $U_s = 3U_{mf}$

denotes the minimum fluidization velocity. Bed expansion in water was insensitive to mesh size, while for air the coarse grid slightly overpredicted expansion; medium and fine meshes produced nearly identical results. Figures 2 compare the results, confirming the medium mesh selection.

Table 2: CFD-DEM simulation parameters

Parameter	Value	Unit
Cell geometry		
Column height, H	0.45	m
Column diameter, D	0.14	m
Solid phase		
Large particle diameter, d_1	4	mm
Small particle diameter, d_2	3	mm
Particles density, ρ_p	2230	$\mathrm{kg\,m^{-3}}$
Young's modulus, E	1.0×10^7	Pa
Poisson's ratio, ν	0.3	-
Restitution coefficient, e	0.6	-
Sliding friction coefficient, μ_s	0.2	-
Rolling friction coefficient, μ_r	0.002	-
Initial bed height, H_i	0.093	m
Initial solid holdup, α_s	0.626	-
Liquid phase		
Liquid density, ρ_w	1000	$\mathrm{kg\,m^{-3}}$
Liquid viscosity, μ_w	0.001	Pa·s
Gas density, ρ_a	1.2	$\mathrm{kg\,m^{-3}}$
Gas viscosity, μ_a	1.9×10^{-5}	Pa·s
Simulation setup		
CFD time step, Δt_{CFD}	5.0×10^{-6}	s
DEM time step, Δt_{DEM}	2.0×10^{-5}	s
Simulation time	20	s

V. RESULTS AND DISCUSSION

In this section, gas–solid and liquid–solid fluidized beds are compared under similar conditions using bed expansion, pressure drop, solid fraction profiles, Lacey Mixing Index, and particle trajectories to evaluate fluidization behavior.

A. Fluidization behavior

The fluidization behavior was studied for air and water as fluidizing media by varying the superficial velocity. For each fluid, six 20 seconds simulations were performed at $0.5U_{mf}$, U_{mf}, $1.5U_{mf}$, $2.0U_{mf}$, $2.5U_{mf}$, and $3.0U_{mf}$. The minimum fluidization velocity was first estimated using the Wen and Yu (1966) correlation. Velocity ranges were scaled for each medium according to the calculated U_{mf}.

Bed performance was evaluated primarily through bed expansion, which depends on fluid velocity, particle properties, and geometry. Figures 3 and 4 show particle distributions at $3U_{mf}$. In water, the bed expanded uniformly with stable particle suspension due to higher density and viscosity, which enhance drag and promote homogeneous mixing. In air, the bed expanded more and exhibited vigorous particle motion, a result of lower density and viscosity producing a more extended fluidization regime.

B. Pressure drop

Before fluidization, the bed is in a fixed (packed) state, and the variation of pressure drop (per unit bed height) is related to the superficial velocity as given by the Ergun's equation [12]:

$$\frac{\Delta P}{H_e} = \frac{150(1-\alpha_f)^2 \mu_f U_s}{\alpha_f^3 d_i^2} + \frac{1.75(1-\alpha_f)\rho_f U_s^2}{\alpha_f^3 d_i}, \quad (6)$$

where ΔP is the pressure drop, H_e is the bed height, μ_f is the fluid viscosity and d_i is calculated using the Sauter mean diameter. Figures 5 and 6 present a comparison between the numerical and the analytical pressure drop calculated using Equation (6). The minimum fluidization velocity, which is shown as $U_{\mathrm{mf,th}}$ in the above figures, was determined using the empirical correlation proposed by Wen and Yu [13], expressed as:

$$U_{mf} = \frac{\mu_f}{\rho_f d_i}\left(\sqrt{33.7^2 + 0.0408\,Ar} - 33.7\right) \quad (7)$$

where Ar represents the Archimedes number, defined as

$$Ar = \frac{g\, d_i^3\, \rho_f\, (\rho_p - \rho_f)}{\mu_f^2}. \quad (8)$$

Some difference in the numerical and theoretical prediction of the minimum fluidization velocity is apparent from the figures, which is expected due to the assumptions involved in theoretical estimates. In the theoretical prediction in Figures 5 and 6, the pressure drop is assumed to remain constant once the minimum fluidization condition is reached.

At the point of minimum fluidization, the upward fluid flow lifts the particles, generating a drag force that balances their effective weight (i.e. the weight reduced by buoyancy). Consequently, the pressure drop across the bed equals the effective weight of the suspended particles and can be expressed as:

$$\Delta P = H_e(\rho_p - \rho_f)(1-\alpha_f)g. \quad (9)$$

This expression is derived from a simplified force balance on a uniform bed at the onset of fluidization. The bed height used here is the initial bed height, which is nearly equal to

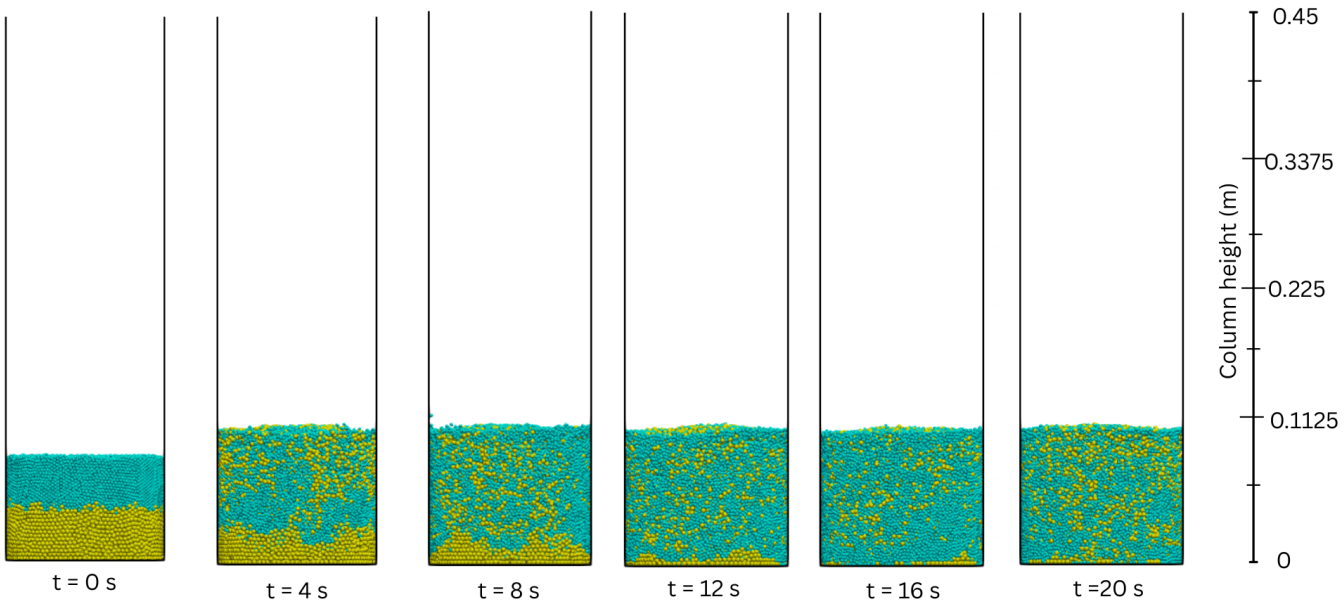

Figure 3: **Qualitative results showing fluidization behavior, including bed height and particle mixing, at different time instances for a superficial velocity of $U_s = 3U_{mf}$ in the water case. The system contains two types of particles with radii $r_1 = 1.5$ mm and $r_2 = 2.0$ mm, both having the same density and a mass of 1kg each.**

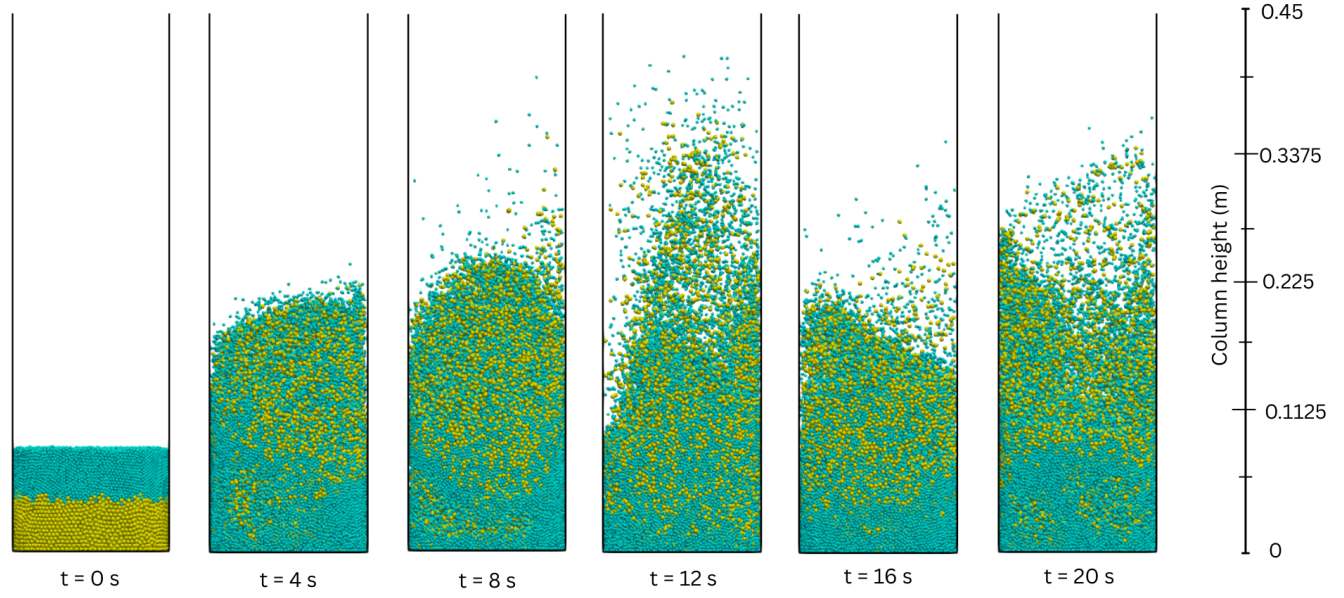

Figure 4: **Qualitative results showing fluidization behavior, including bed height and particle mixing, at different time instances for a superficial velocity of $U_s = 3U_{mf}$ in the air case. The system contains two types of particles with radii $r_1 = 1.5$ mm and $r_2 = 2.0$ mm, both having the same density and a mass of 1kg each.**

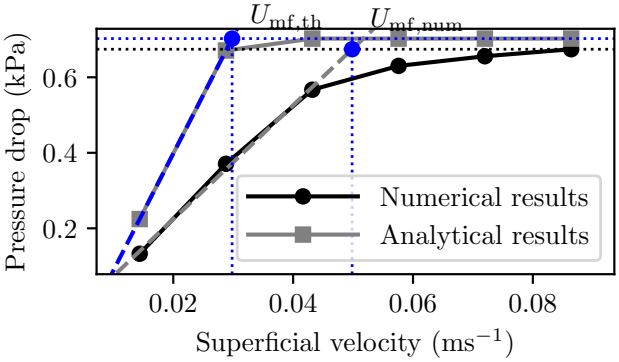

Figure 5: **Comparison of pressure drop versus superficial velocity from CFD–DEM simulations and theoretical correlations for the water case.**

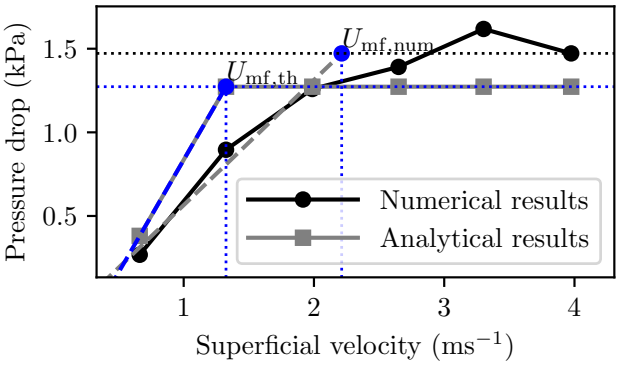

Figure 6: **Comparison of pressure drop versus superficial velocity from CFD–DEM simulations and theoretical correlations for the air case.**

the bed height at minimum fluidization velocity. As shown in Figures 5 and 6 for the numerical prediction of pressure drop, in both air and water-fluidized beds, the pressure drop rose with superficial velocity in the fixed-bed regime until reaching the minimum fluidization velocity, where drag balances bed weight. Beyond U_{mf}, the bed expanded and ΔP remained nearly constant. Due to higher density and viscosity, water achieved fluidization at a lower U_{mf} than air. Fluidization ΔP of 0.703kPa and 1.472kPa was found using simulations for water and air, respectively. These correspond to errors of 4.08% (water) and 15.6% (air) compared to theoretical predictions (from Equation (**??**)), showing good agreement, especially for the liquid system.

C. Particle Mixing

Particle mixing, a key factor in fluidized bed performance, was examined in gas and water systems using colored-particle tracking at $U_s = 3U_{mf}$ for 20 s. Both cases started from the same packed configuration. Visualizations (Figures 3 and 4) show that particle spread rate and extent depend strongly on the fluidizing medium. Mixing was quantified using the Lacey mixing index (LMI) [14]. As

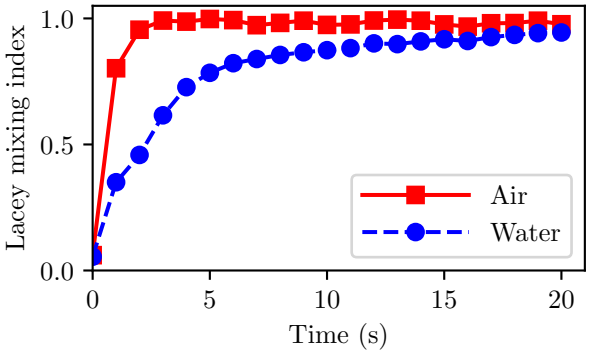

Figure 7: **Evolution of the Lacey mixing index.**

shown in Figure 7, water-fluidized beds exhibit gradual, steady LMI growth, indicating progressive mixing. In contrast, the air case shows rapid early mixing, followed by a slower approach to uniformity. These results confirm that fluid density and viscosity significantly influence mixing dynamics and efficiency.

VI. CONCLUSIONS

A coupled CFD–DEM framework was employed to study binary particle fluidization in a 3D cylindrical bed using air and water as fluidizing media. Under the same geometry, fluidizing velocities were adjusted to account for differences in fluid properties. The effects of these properties on bed expansion, pressure drop, and particle mixing were then evaluated and compared for both fluids.

Fluid properties were found to strongly influence the fluidization regime. Water's higher density and viscosity produced uniform expansion, stable pressure profiles, and confined particle motion, while air yielded larger bed expansion, greater particle mobility, and stronger fluctuations. Simulated minimum fluidization velocity and pressure drop agreed well with theoretical predictions, confirming model accuracy.

Mixing, quantified via the Lacey mixing index, improved with increasing superficial velocity, with the fluid medium influencing both rate and extent. These results underscore the role of fluid selection in optimizing mixing performance and mitigating segregation in multiphase reactors.

This work provides quantitative insights into fluid–solid interactions for both liquid–solid and gas–solid systems, offering a basis for improved design and operation of fluidized beds.

ACKNOWLEDGEMENTS

RN thanks the Ministry of Education, Government of India, for scholarship support during his PhD. The authors acknowledge the National Supercomputing Mission for computing resources on 'PARAM Himalaya' at IIT Mandi, supported by C-DAC, MeitY, and DST, Government of India.

NOMENCLATURE

Symbol	Description	Unit
C_d	Drag coefficient of solid particle	—
d_i	Particle diameter	m
D	Column diameter	m
E	Young's modulus	Pa
e	Coefficient of restitution	—
$\mathbf{F}_d$	Fluid drag force	N
$\mathbf{F}_c$	Contact force	N
$\mathbf{g}$	Acceleration due to gravity	$\mathrm{m\,s^{-2}}$
H	Column height	m
H_e	Height of bed	m
$\mathbf{I}_i$	Moment of inertia of particle i	$\mathrm{kg\,m^2}$
$\mathbf{K}_{sl}$	Momentum exchange term	$\mathrm{kg\,m^{-3}\,s^{-1}}$
m_i	Particle mass	kg
p	Pressure	Pa
t	Time	s
$\mathbf{T}_c$	Net moment due to contact forces	$\mathrm{N\,m}$
$\mathbf{T}_{fi}$	Moment due to fluid–particle interaction	$\mathrm{N\,m}$
$\mathbf{u}_f$	Fluid velocity	$\mathrm{m\,s^{-1}}$
U_s	Superficial velocity	$\mathrm{m\,s^{-1}}$
$U_{\mathrm{mf,num}}$	Simulation minimum fluidization velocity	$\mathrm{m\,s^{-1}}$
$U_{\mathrm{mf,th}}$	Theoretical minimum fluidization velocity	$\mathrm{m\,s^{-1}}$
$\mathbf{U}_r$	Relative velocity (particle–fluid)	$\mathrm{m\,s^{-1}}$
Greek letters		
α_f	Fluid volume fraction	—
α_s	Initial solid holdup	—
β	Momentum exchange exponent	—
Δt	Simulation time step size	s
μ_f	Fluid dynamic viscosity	$\mathrm{Pa\,s}$
μ_w	Liquid viscosity	$\mathrm{Pa\,s}$
μ_a	Gas viscosity	$\mathrm{Pa\,s}$
μ_s	Sliding friction coefficient	—
μ_r	Rolling friction coefficient	—
ν	Poisson's ratio	—
ρ_f	Fluid density	$\mathrm{kg\,m^{-3}}$
ρ_a	Gas density	$\mathrm{kg\,m^{-3}}$
ρ_p	Particle density	$\mathrm{kg\,m^{-3}}$
τ_f	Fluid shear stress tensor	Pa
ω_i	Particle angular velocity	$\mathrm{rad\,s^{-1}}$

REFERENCES

[1] Islam, Md Tariqul and Nguyen, Anh V. Liquid-assisted irregular coarse particle fluidization in a fluidized bed flotation cell: Bed of low-density versus high-density particles. *Minerals Engineering*, 201:108153, 2023.

[2] Zhouzun Xie, Shuai Wang, and Yansong Shen. CFD–DEM study of segregation and mixing characteristics under a bi-disperse solid-liquid fluidised bed. *Advanced Powder Technology*, 32(11):4078–4095, 2021.

[3] Fria Hossein, Massimiliano Materazzi, Matteo Errigo, Panagiota Angeli, and Paola Lettieri. Application of ultrasound techniques in solid–liquid fluidized bed. *Measurement*, 194:111017, 2022.

[4] Md Shakhaoath Khan, Subhasish Mitra, Swapnil Ghatage, Zhengbiao Peng, Elham Doroodchi, Behdad Moghtaderi, Jyeshtharaj B Joshi, and Geoffrey M Evans. Pressure drop and voidage measurement in solid–liquid fluidized bed: Experimental, mathematical and computational study. *Chemeca 2016: Chemical Engineering-Regeneration, Recovery and Reinvention*, pages 1019–1030, 2016.

[5] Jian Peng, Wei Sun, Haisheng Han, Le Xie, and Yao Xiao. Experimental and numerical simulation study on the hydrodynamic characteristics of spherical and irregular-shaped particles in a 3d liquid-fluidized bed. *Korean Journal of Chemical Engineering*, 39(11):3165–3176, 2022.

[6] Hamed Hoorijani, Behrad Esgandari, Reza Zarghami, Rahmat Sotudeh-Gharebagh, and Navid Mostoufi. Comparative CFD–DEM study of flow regimes in spout-fluid beds. *Particuology*, 85:323–334, 2024.

[7] Youjun Lu, Jikai Huang, Pengfei Zheng, and Dengwei Jing. Flow structure and bubble dynamics in supercritical water fluidized bed and gas fluidized bed: A comparative study. *International Journal of Multiphase Flow*, 73:130–141, 2015.

[8] Rongtao Feng, Junguo Li, Zhonghu Cheng, Xin Yang, and Yitian Fang. Influence of particle size distribution on minimum fluidization velocity and bed expansion at elevated pressure. *Powder Technology*, 320:27–36, 2017.

[9] Zhenjiang Zhao, Ling Zhou, Ling Bai, Wanning Lv, and Ramesh K Agarwal. Effects of particle diameter and inlet flow rate on gas–solid flow patterns of fluidized bed. *ACS omega*, 8(7):7151–7162, 2023.

[10] Shijiao Li, Peng Zhao, Ji Xu, Li Zhang, and Junwu Wang. Cfd–dem simulation of polydisperse gas-solid flow of geldart a particles in bubbling micro-fluidized beds. *Chemical Engineering Science*, 253:117551, 2022.

[11] Md Tariqul Islam and Anh V Nguyen. A numerical study with experimental validation of liquid-assisted fluidization of particle suspensions in a HydroFloat cell. *Minerals Engineering*, 134:176–192, 2019.

[12] Feng-Jehng Wang, Suming Chen, Perng-Kwei Lei, and Chung-Hsing Wu. Effects of pressure drop and superficial velocity on the bubbling fluidized bed incinerator. *Journal of Environmental Science and Health, Part A*, 42(14):2147–2158, 2007.

[13] Ramesh Timsina, Rajan Kumar Thapa, Britt Margrethe Emilie Moldestad, and Marianne Sørflaten Eikeland. Effect of particle size on flow behavior in fluidized beds. 2019.

[14] P.M.C Lacey. Developments in the theory of particle mixing. *Journal of Applied Chemistry*, 4(5):257–268, 1954.